

Inner edge of neutron-star crust with SLy effective nucleon-nucleon interactions

F. Douchin¹, P. Haensel^{1,2,3}

¹*Centre de Recherche Astronomique de Lyon,
Ecole Normale Supérieure de Lyon, 46, allée d'Italie,
69364 Lyon, France*

²*N. Copernicus Astronomical Center,
Polish Academy of Sciences, Bartycka 18,
00-716 Warszawa, Poland*

³*Département d'Astrophysique Relativiste et de Cosmologie,
UMR 8629 du CNRS, Observatoire de Paris,
F-92195 Meudon Cedex, France*

October 29, 2018

to be published in Physics Letters B

Abstract

The boundary between the solid crust, assumed to be in complete thermodynamic equilibrium (cold catalyzed matter), and the liquid core of a neutron star is studied using Skyrme SLy effective N-N interactions. An approximate value of the density at the inner edge of the crust is obtained from the threshold for the instability of homogeneous *npe* matter with respect to small periodic density perturbations. Calculations of the bottom layer of the crust are performed within the Compressible Liquid Drop Model. Spherical nuclei are energetically preferred over exotic ones (cylinders, plates, tubes, bubbles), down to the inner edge of the crust, found at $\rho_{\text{edge}} = 0.08 \text{ fm}^{-3}$.

Key words: Dense matter. Neutron stars.

PACS numbers: 97.60.Jd, 21.65.+f, 95.30.Cq

The solid crust of a neutron star plays an important role in neutron star evolution and dynamics. It insulates thermally neutron star surface from its hot liquid interior, and therefore plays an essential role in neutron star cooling. It can build-up stresses, leading to instabilities responsible for the glitches in pulsar timing. Moreover, it can support non-axial deformations which, combined with rapid rotation, could make neutron star a source of continuous gravitational radiation.

The mass of the neutron-star crust depends sensitively on the density of its inner edge and on the neutron-star matter equation of state. Recent calculations of this quantity

[17, 11, 18, 8] give $\rho_{\text{edge}} \simeq 0.08 - 0.10 \text{ fm}^{-3}$, substantially lower than the estimate close to the normal nuclear density $\rho_0 = 0.16 \text{ fm}^{-3}$, derived in the classical paper of Baym et al. [1]. Some theoretical calculations predict exotic distributions of nuclear matter (rods, plates, etc.) within the bottom layers of the crust [17, 11, 9]. However, the presence of exotic nuclei depends on the effective nucleon-nucleon (N-N) force used; for some forces, spherical nuclei are present down to the inner edge of the crust [17, 8]. Presence of exotic nuclei would lead to different transport and elastic properties of the crust, compared to the standard case of a Coulomb crystal formed by spherical nuclei [17, 13]. This, in turn, would have important consequences for dynamics and evolution of neutron star.

In order to make calculations of the structure of the bottom layers of the neutron-star crust feasible, one has to use an effective N-N interaction. Frequently used in astrophysical applications SkM* force was constructed to provide a consistent description of isovector properties of nuclei (giant dipole resonances) [5], and seems thus to be particularly suitable for the description of neutron rich nuclei. However, this as well as many other existing effective N-N interactions were fitted to the properties of laboratory atomic nuclei, with $(N - Z)/A < 0.3$, while in the bottom layers of neutron-star crust one expects $(\rho_n - \rho_p)/\rho \gtrsim 0.8$. In view of this, application of these effective N-N interactions to the bottom layers of a neutron-star crust involves a rather risky extrapolation to strongly asymmetric nucleon matter. In order to remove a part of this uncertainty, modifications of effective N-N forces, to make them consistent with microscopic calculations of neutron matter, have been applied. Such a procedure was used in seventies to obtain the Sk1' force [4], via a rather *ad hoc* modification of the Sk1 force constructed originally by Vautherin and Brink [3] to describe terrestrial nuclei. In this way, it became consistent with energy per nucleon of neutron matter calculated by Siemens and Pandharipande [15]. Later, generalized types of the Skyrme interaction, FPS [12] and FPS21 [18], with larger number of fitted parameters and more general density dependence, were derived by fitting the temperature and density dependent energies per baryon of nuclear and neutron matter obtained in microscopic calculations of Friedman and Pandharipande [10].

Recently, a new set of the Skyrme-type effective N-N interaction has been derived, based on an approach which may be more appropriate, as far as the applications to a very neutron rich matter are concerned [6, 7]. Relevant additional experimental items concerning neutron rich nuclei (isovector effective masses), constraints of spin stability, and requirement of consistency with the UV14+VIII equation of state (EOS) of dense neutron matter of Wiringa et al. [20] for $\rho_0 \leq \rho \leq 1.5 \text{ fm}^{-3}$, were combined with general procedure of fitting the properties of doubly magic nuclei. This procedure led to a set of the SLy (Skyrme Lyon) models, which - due to the emphasis put on their neutron-excess dependence - seem to be particularly suitable for the calculations of the properties of neutron-star crust.

In the present Letter, we calculate the structure of the bottom layer of the neutron-star crust, and the density at its inner edge, ρ_{edge} , using the SLy models of effective N-N interaction, and compare our results with those obtained using older Skyrme-type forces, SkM* and Sk1'. The parameters of the SLy forces used in the present calculations, together with those of the SkM* and Sk1' models, are given in Table 1. The SLy4 interaction is a basic SLy force. The SLy7 model has been obtained following the most ambitious fitting procedure, in which spin-gradient terms and center of mass correction term were both included in the Skyrme energy functional [7].

Recent calculations show that neutron-star matter (both liquid and solid) close to the crust-liquid core interface contains only a few percent of protons. Therefore, an effective N-N interaction used for the calculation of the crust-liquid transition should, in the first place, yield a realistic description of pure neutron matter at subnuclear density. As we do not have a direct access to the EOS of pure neutron matter at subnuclear densities, results of precise numerical calculations of the ground state at $\rho < \rho_0$, carried out using modern many-body theories and the best *bare* N-N hamiltonians, are to be used as an ersatz of such experimental data [18].

The SLy forces have been constructed as to be consistent with the UV14+UVII model of Wiringa et al. [20] of neutron matter above ρ_0 [6, 7]. It is therefore of interest to see how well these effective N-N forces reproduce the UV14+UVII model of neutron matter at subnuclear densities.

In Fig. 1 we have plotted the energy per neutron, e , versus neutron density, $\rho < \rho_0$, for the SLy4 and SLy7 effective N-N interactions. The filled squares correspond to realistic UV14+UVII model of neutron matter, and were taken from Table III of Wiringa et al. [20]. The agreement of the SLy4, SLy7 curves with the neutron matter EOS of the UV14+VII model of Wiringa et al. [20] is very good. This is not the case for older Skyrme forces, Sk1' and SkM*.

In what follows, a mixture of neutrons, protons, and electrons will be referred to as *npe* matter. An electrically neutral *npe* matter in beta equilibrium corresponds to neutron-star matter at $\rho \sim \rho_0$. At a given ρ , the ground state of a homogeneous *npe* matter corresponds to the minimum of the energy density $E(\rho_n, \rho_p, \rho_e) = E_0$, under the constraints of fixed baryon density and electric charge neutrality, $\rho_p + \rho_n = \rho$ and $\rho_e = \rho_p$, respectively. This implies beta equilibrium between the matter constituents and ensures vanishing of the first variation of E due to small perturbations $\delta\rho_j(\mathbf{r})$ (where $j = n, p, e$) of the equilibrium solution (under the constraints of constant total nucleon number, $A = \rho V$, and global charge neutrality within the volume V of the system). However, this does not guarantee the stability of the spatially homogeneous state of the *npe* matter, which requires that the second variation of E (quadratic in $\delta\rho_j$) be positive.

Our expression for the energy functional of slightly inhomogeneous neutron-star matter has been calculated using the semi-classical Extended Thomas-Fermi (ETF) treatment of the kinetic and the spin-gradient terms in nucleon contribution to E [2]. Assuming that the spatial gradients are small, we keep only the quadratic gradient terms in the ETF expressions. Our approximation is justified by the fact that characteristic wavelengths of periodic perturbations turn out to be much larger than the internucleon distance. With these approximations, the change of the energy (per unit volume) implied by the density perturbations can be expressed, keeping only second order terms [1, 18],

$$E - E_0 = \frac{1}{2} \int \frac{d\mathbf{q}}{(2\pi)^3} \sum_{i,j} F_{ij}(\mathbf{q}) \delta\rho_i(\mathbf{q}) \delta\rho_j(\mathbf{q})^* , \quad (1)$$

where we used the Fourier representation

$$\delta\rho_j(\mathbf{r}) = \int \frac{d\mathbf{q}}{(2\pi)^3} \delta\rho_j(\mathbf{q}) e^{i\mathbf{q}\mathbf{r}} . \quad (2)$$

The hermitian $F_{ij}(\mathbf{q})$ matrix determines the stability of the uniform state of equilibrium of the *npe* matter with respect to the spatially periodic perturbations of wavevector \mathbf{q} . Due

to the isotropy of the homogeneous equilibrium state of the npe matter, F_{ij} depends only on $|\mathbf{q}| = q$. In the case of Skyrme-type forces, the matrix elements F_{ij} can be calculated analytically, as explicit functions of the equilibrium densities and q , and are composed of compression (local), curvature (gradient), and Coulomb components [1, 18].

The condition for the F_{ij} matrix to be positive definite is equivalent to the requirement that the determinant of the F_{ij} matrix be positive [18]. At each density ρ , one has thus to check the condition $\det[F_{ij}(q)] > 0$. Let us start with some ρ , at which $\det[F_{ij}(q)] > 0$ for any q . By decreasing ρ , we find eventually a wavenumber Q at which stability condition is violated for the first time; this happens at some density ρ_Q . For $\rho < \rho_Q$ the homogeneous state is no longer the ground state of the npe matter since it is unstable with respect to small periodic density modulations.

We get $\rho_Q = 0.079 \text{ fm}^{-3}$ for both SLy4 and SLy7 forces, to be compared with 0.075 fm^{-3} and 0.101 fm^{-3} for the SkM* and Sk1' forces, respectively. The instability at ρ_Q signals a phase transition with a loss of translational symmetry of the npe matter, and appearance of nuclear structures. Calculations performed previously with Skyrme forces indicate that $\rho_Q \simeq \rho_{\text{edge}}$ [18]. The differences between the values of ρ_Q between four forces are correlated with differences in the density behavior of nucleon chemical potentials, whose density derivatives enter the stability matrix F_{ij} [18]. In Fig.2 we plot the values of μ_n and μ_p for all four Skyrme forces considered, versus nucleon density ρ , for the npe matter in beta equilibrium. In the relevant density region, $\rho \sim \frac{1}{2}\rho_0$, one notices very good agreement between the values of μ_p . The relative differences in the values of μ_n , and in particular in the slopes of the $\mu_n(\rho)$ curves are much larger. The slope of $\mu_n(\rho)$ for the SkM* force is the highest, and that for the Sk1' force the lowest, at $\rho \simeq \frac{1}{2}\rho_0$. Notice that the slope of μ_n for the Sk1' is quite similar to those obtained in [18] for the FPS and FPS21 forces (see Fig.5 of [18]). Qualitatively, the higher the slope of μ_n , the lower the value of ρ_Q (c.f., [18]).

Nuclear structures in bottom layers of neutron-star crust were described using the Compressible Liquid Drop Model (CLDM) of nuclei [1, 21, 22, 23]. Within the CLDM, one is able to separate bulk, surface, and Coulomb contributions to total energy density, E . Electrons are assumed to form an uniform Fermi gas, and yield the rest and kinetic energy contribution, denoted by E_e . Within CLDM, total energy density of the inner neutron-star crust is given by

$$E = E_{\text{N,bulk}} + E_{\text{N,surf}} + E_{\text{Coul}} + E_e . \quad (3)$$

Here, $E_{\text{N,bulk}}$ is the bulk contribution of nucleons, which does not depend on the shape of nuclear structures. However, both $E_{\text{N,surf}}$ and E_{Coul} do depend on the shape of nuclear structures, formed by denser nuclear matter and the less dense neutron gas (detailed description of the calculation of $E_{\text{N,surf}}$ and E_{Coul} for the SLy forces was presented in [23]; our results for the nuclear surface and curvature properties for SLy forces will be described in detail elsewhere [24]). We restricted ourselves to three shapes of the nuclear matter - neutron gas interface: spherical, cylindrical, and plane. Consequently, we considered five types of nuclear structures: spheres of nuclear matter in neutron gas, cylinders of nuclear matter in neutron gas (rods), plane slabs of nuclear matter in neutron gas, cylindrical holes in nuclear matter filled by neutron gas (tubes), and spherical holes in nuclear matter filled by neutron gas (bubbles). In view of a significant neutron excess, the interface includes neutron skin, formed by neutrons adsorbed onto the nuclear matter surface. In view of a finite thickness of nuclear surface, the definition of its spatial location is a matter of convention. Here, we

defined it by the radius of the equivalent constant density proton distribution, R_p , which determines thus the radius of spheres, bubbles, cylinders and tubes, and the half-thickness of plane nuclear matter slabs. The neutron radius, R_n , was defined by the condition that it yields a squared-off neutron density distribution with constant neutron densities, which are equal to the real ones far from the nuclear matter – neutron gas interface, reproduces actual numbers of neutrons. The thickness of the neutron skin is then defined as $R_n - R_p$, R_p being defined in a similar manner as R_n . The nuclear surface energy term, $E_{N,\text{surf}}$, gives the contribution of the interface between neutron gas and nuclear matter; it includes contribution of neutron skin [21, 16, 22]. In the case of spherical and cylindrical interface, $E_{N,\text{surf}}$ includes curvature correction; the curvature correction vanishes for slabs.

In order to calculate E_{Coul} , we used the Wigner-Seitz approximation. In the case of spheres, bubbles, rods, and tubes, Wigner-Seitz cells were approximated by spheres, and cylinders, of radius R_{cell} . In the case of slabs, Wigner-Seitz cells were bounded by planes, with R_{cell} being defined as the half-distance between plane boundaries of the cell. At given average nucleon density, ρ , and for an assumed shape of nuclear structures, the energy density was minimized with respect to thermodynamic variables, under the condition of an average charge neutrality [21, 22, 23]. Our results for $E(\rho)$ for the SLy4 force, together with the energy density of the uniform *npe* matter, are displayed in Fig. 3. For the sake of convenience, energy densities has been shown after subtracting the value of the energy density of the bulk nuclear matter - neutron gas system (charge neutral and in beta equilibrium), $\Delta E(\rho) \equiv E(\rho) - E_{\text{bulk}}(\rho)$. Spherical nuclei turn out to be energetically preferred over other nuclear shapes, and also over homogeneous *npe* matter, down to $\rho_{\text{crit}} = 0.077 \text{ fm}^{-3}$. Therefore, within our set of possible nuclear shapes, the ground state of neutron-star crust contains spherical nuclei, down to its bottom edge.

As was already noticed in [28, 29, 17], exotic nuclei will be present only if the filling fraction, u , is large enough. For a given neutron excess, introducing finite size (Coulomb and surface) effects increases the value of u . This increase of u is larger when the surface tension is larger, the finite-size effect being roughly proportional to it. Therefore, the larger the surface tension, the more likely the exotic nuclei are to appear. For all Skyrme forces we have studied so far, our results are in agreement with this qualitative rule. In particular, at the proton fraction $\sim 5 - 8\%$ the surface tension for the SkM* and SLy forces, for which exotic nuclei do not appear, is much smaller than for the Sk1' model, for which exotic nuclei do appear.

Actually, under conditions of thermodynamic equilibrium, transition from the crust to the uniform liquid takes place at a constant pressure, and is accompanied by a density jump (first order phase transition). Using Maxwell construction, we find that the edge of the crust has density $\rho_{\text{edge}} = 0.076 \text{ fm}^{-3}$, and coexists there with uniform *npe* matter of the density higher by $\Delta\rho/\rho_{\text{edge}} = 1.4\%$. Therefore, crust-liquid core transition is a very weak first-order phase transition; it takes place at $P_{\text{edge}} = 0.34 \text{ MeV}/\text{fm}^3$.

Geometrical parameters characterizing the bottom layers of the crust are shown in Fig. 4. Here, R_p is the proton radius corresponding to the equivalent squared proton distribution within nuclei, R_{cell} is the radius of the Wigner-Seitz cell, and u is the fraction of volume occupied by nuclear matter (equal to that occupied by protons). The crust-liquid core transition takes place not because nuclei grow in size, but rather because they become closer and closer. The filling fraction u grows rapidly for ρ approaching ρ_{edge} , from only

5 % at $\rho = 0.04 \text{ fm}^{-3}$ to nearly 30 % at ρ_{edge} . Still, less than 30% of the volume is filled by nuclear matter at the crust-liquid core transition point. Our maximum filling factor is significantly larger than the limiting value of 0.2 for spherical nuclei phase, derived by Oyamatsu et al. [27] using general considerations involving surface and Coulomb energy. This is due to the curvature corrections, included in our formula for $E_{\text{N,surf}}$ and absent in the model of Oyamatsu et al. [27]. Curvature tension is particularly important near the crust-liquid transition point, where the surface tension is very small. If we neglect the curvature term in surface energy, we find maximum u for nuclei of about 0.2, consistent with Oyamatsu et al. [27]. Finally, let us mention that no proton drip occurs in the ground state of the crust.

More detailed information on neutron-rich nuclei, present in the ground state of the bottom layers of neutron-star crust with $\rho \gtrsim \frac{1}{3}\rho_0$, can be found in Fig. 5. Number of nucleons in a nucleus, A , grows monotonically, and reaches about 600 at the edge of the crust. However, the number of protons changes rather weakly, from $Z \simeq 40$ near neutron drip, to $Z \simeq 50$ near the edge of the crust. Our results for Z of spherical nuclei are similar to those obtained in [11, 14], but are somewhat higher than those obtained using a relativistic mean-field model in [9]. An interesting quantity is the number of neutrons forming neutron skin, $N_{\text{n,surf}}$. For $\rho > \frac{1}{3}\rho_0$, we find that $N_{\text{n,surf}}$ decreases with increasing ρ , despite an increase of nuclear radius. This behavior is due to the fact, that neutron densities outside and inside nuclei become more and more alike, while thickness of neutron skin decreases, with increasing ρ , for $\rho > \frac{1}{3}\rho_0$.

Near the bottom of the crust, spherical nuclei are very heavy, $A \sim 300 - 500$, and doubts concerning their stability with respect to deformation and fission arise. An approximate condition for fission in dense neutron-star matter is $R_p/R_{\text{cell}} \gtrsim 1/2$ [16]; this condition is fulfilled near the edge of the crust, Fig. 4. However, curvature terms in $E_{\text{N,surf}}$ and E_{Coul} , which were not included in generalized Bohr-Wheeler condition of [16], as well as shell correction to E [26], stabilize large spherical nuclei. Clearly, the problem of stability of spherical nuclei near the bottom of neutron-star crust deserves further investigation. In any case, however, forming rod-like nuclei in the ground state of neutron-star crust seems to be excluded by the energetical arguments, Fig. 3.

In the CLDM approximation with SLy4 force, uniform npe matter is present in the ground state of the neutron-star interior at the density exceeding $\rho_{\text{liq}} = 0.077 \text{ fm}^{-3}$. Comparing the value of ρ_{liq} with ρ_Q , we have an independent test of precision of our CLDM calculations. The relative difference between these two quantities is less than 3%, which is of the order-of-magnitude of the relative density jump in the crust - liquid core transition, obtained within the CLDM. For the SLy4 force, the crust - liquid core transition takes thus place at half of the normal nuclear density, and very similar value is obtained for the SLy7 force.

The structure of the ground state of neutron-star interior at subnuclear densities, determined in this Letter for the SLy4 force, implies that the bottom layer of the neutron star crust is a three-dimensional Coulomb crystal, with spherical nuclei in the lattice sites, the edge of the crystal being located at $\rho_{\text{edge}} \simeq 0.08 \text{ fm}^{-3}$.

We combined the SLy4 EOS of the inner crust with that of the liquid core, getting in this way a physically consistent, unified description of the neutron star interior beyond neutron drip. As for the outer crust, we have chosen the EOS of Haensel and Pichon [25], in

which maximum use of recent experimental information on neutron rich nuclei was made. For neutron star with canonical mass of $1.4 M_{\odot}$, the crust contains $\Delta M_{\text{crust}}/M = 1.2\%$ of the total stellar mass, and its relative contribution to the total moment of inertia is $\Delta I_{\text{crust}}/I = 2.6\%$. The corresponding values for the FPS neutron star model are some 30% lower, despite larger value of $\rho_{\text{edge}}(\text{FPS}) = 0.10 \text{ fm}^{-3}$. It turns out, however, that $P_{\text{edge}}(\text{FPS}) \simeq P_{\text{edge}}(\text{SLy4})$, because the FPS EOS near ρ_{edge} is significantly softer than the SLy4 one. The difference in the $\Delta M_{\text{crust}}/M$ for both models can thus be explained by the difference in the $R^4(1 - 2GM/Rc^2)$ factor appearing in an approximate expression for ΔM_{crust} [17]; the FPS neutron star of $1.4 M_{\odot}$ is more compact than the SLy4 one. Similar arguments can be used to explain the difference between the $\Delta I_{\text{crust}}/I$ values for the SLy4 and FPS forces (see [17] for the approximate formula to be used). However, the most important difference between the SLy4 and the FPS crusts is that in our case the whole crust, down to its bottom edge, is a Coulomb crystal, while in the FPS case the bottom layer, constituting about half of the crust mass, contains nonstandard nuclear shapes (rods, plates, tubes, bubbles), and therefore has elastic and transport properties very different from those of a three-dimensional Coulomb crystal [13]. Finally, presence of a Coulomb crystal is also relevant for the crust - liquid core boundary condition in rotating neutron stars.

ACKNOWLEDGMENTS

We are grateful to G. Chabrier and J. Meyer for a critical reading of the preliminary version of the manuscript and for helpful remarks. P.H. acknowledges the hospitality of ENS de Lyon during his stay with the theoretical astrophysics group of CRAL. This work was supported in part by the KBN grant No. 2 P03D 014 13 and by the French CNRS/MAE program Jumelage Astronomie France-Pologne. During his visits at DARC, P.Haensel was supported by the PAST professorship of French MENRT.

References

- [1] G. Baym, H.A. Bethe, C.J. Pethick, Nucl. Phys. A **175** (1971) 225
- [2] M. Brack, B.K. Jennings, Y.H. Chu, Phys. Lett. B **65** (1976) 1
- [3] Vautherin, D., Brink, D.M., Phys. Lett. B **32** (1970) 149
- [4] J.M. Lattimer, D.G. Ravenhall, Ap. J. **223** (1978) 314
- [5] J. Bartel, P. Quentin, M. Brack, C. Guet, H.B. Håkanson, Nucl. Phys. A **386** (1982) 79
- [6] E. Chabanat, P. Bonche, P. Haensel, J. Meyer, R. Schaeffer, Nucl. Phys. A **627** (1997) 710
- [7] E. Chabanat, P. Bonche, P. Haensel, J. Meyer, R. Schaeffer, Nucl. Phys. A **635** (1998) 231
- [8] K.S. Cheng, C.C. Yao, Z.G. Dai, Phys. Rev. C **55** (1997) 2092

- [9] K. Sumiyoshi, K. Oyamatsu, H. Toki, Nucl. Phys. A **595** (1995) 327
- [10] B. Friedman, V.R. Pandharipande, Nucl. Phys. A **361** (1981) 502
- [11] K. Oyamatsu, Nucl. Phys. A **561** (1993) 431
- [12] V.R. Pandharipande, D.G. Ravenhall, Proc. NATO Advanced Research Workshop on nuclear matter and heavy ion collisions, Les Houches, 1989, eds. M. Soyeur et al. (Plenum, New York, 1989) p.103
- [13] C.J. Pethick, A.Y. Potekhin, Phys. Lett. B **427** (1998) 7
- [14] D.G. Ravenhall, C.D. Bennett, C.J. Pethick, Phys. Rev. Lett. **28** (1972) 978
- [15] P.J. Siemens, V.R. Pandharipande, Nucl. Phys. A **173** (1971) 561
- [16] C.J. Pethick, D.G. Ravenhall, Ann.Rev. Nucl. Part. Sci. **45** (1995) 429
- [17] C.P. Lorenz, D.G. Ravenhall, C.J. Pethick, Phys. Rev. Lett. **70** (1993) 379
- [18] C.J. Pethick, D.G. Ravenhall, C.P. Lorenz, Nucl. Phys. A **584** (1995) 675
- [19] S.L. Shapiro, S.A. Teukolsky, Black Holes, White Dwarfs and Neutron Stars, (Wiley, New York, 1983) sect. 5.7
- [20] R.B. Wiringa, V. Fiks, A. Fabrocini, Phys. Rev. C **38** (1988) 1010
- [21] J.M. Lattimer, C.J. Pethick, D.G. Ravenhall, D.Q. Lamb, Nucl. Phys. A **432** (1985) 646
- [22] C.P. Lorenz, PhD Thesis, University of Illinois, Urbana-Champaign (1991)
- [23] F. Douchin, PhD Thesis, Ecole Normale Supérieure de Lyon (1999)
- [24] F. Douchin, P. Haensel, J. Meyer, Nucl. Phys. A **665** (2000) 419
- [25] P. Haensel, B. Pichon, Astron. Astrophys. **283** (1994) 313
- [26] K. Oyamatsu, M. Yamada, Nucl. Phys. A **578** (1994) 181
- [27] K. Oyamatsu, M. Hashimoto, M. Yamada, Prog. Theor. Phys. **72** (1984) 373
- [28] D.G. Ravenhall, C.J. Pethick, J.R. Wilson, Phys. Rev. Lett. **50** (1983) 2066
- [29] M. Hashimoto, H. Seki, M. Yamada, Prog. Theor. Phys. **71** (1984) 320

Table 1

Parameter values of the Skyrme forces

force	SLy4	SLy7	SkM*	Sk1'
t_0 (MeV fm ³)	-2488.91	-2482.41	-2645.0	-1057.3
t_1 (MeV fm ⁵)	486.82	457.97	410.0	235.9
t_2 (MeV fm ⁵)	-546.39	-419.85	-135.0	-100.00
t_3 (MeV fm ^{3+3σ})	13777.0	13677.0	15595.0	14463.5
σ	$\frac{1}{6}$	$\frac{1}{6}$	$\frac{1}{6}$	1
x_0	0.834	0.846	0.09	0.2885
x_1	-0.344	-0.511	0	0
x_2	-1.000	-1.000	0	0
x_3	1.354	1.391	0	0.2257
W_0 (MeV fm ⁵)	123.0	126.0	130.0	120.0

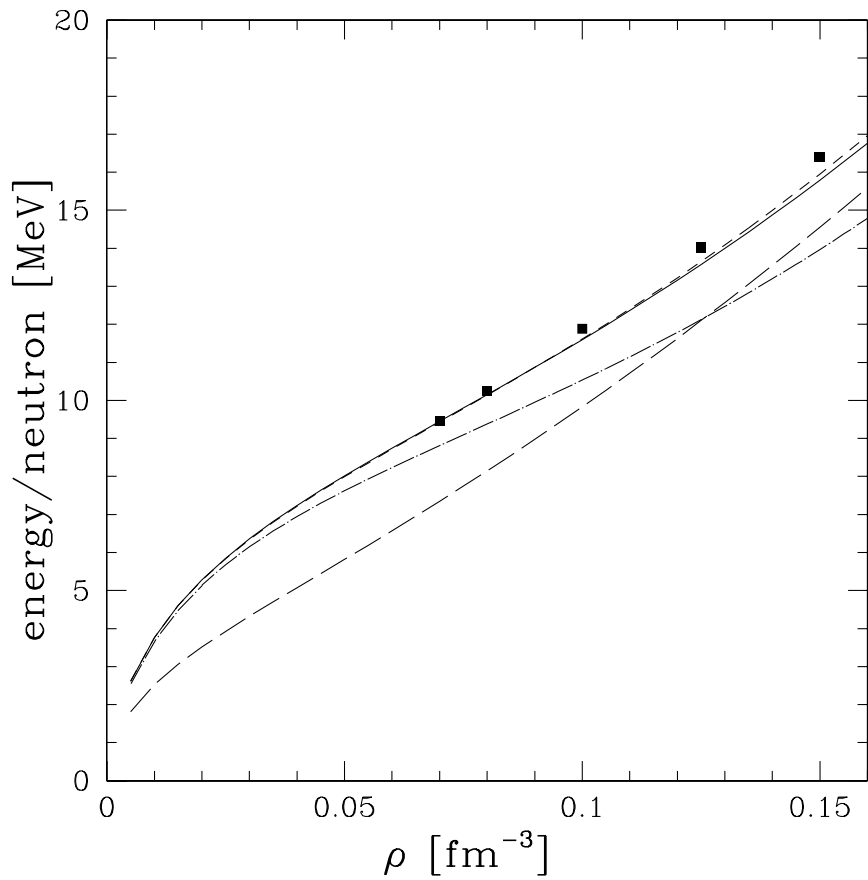


Figure 1:

Energy per neutron versus neutron density for neutron matter. Filled squares: results of Wiringa et al. [20] for the UV14+UVIII model. Solid line: the SLy4 model. Short dashes: the SLy7 model. For the sake of comparison, we show also results obtained for the SkM* (long dashes) and the Sk1' (long dash-dot line) models.

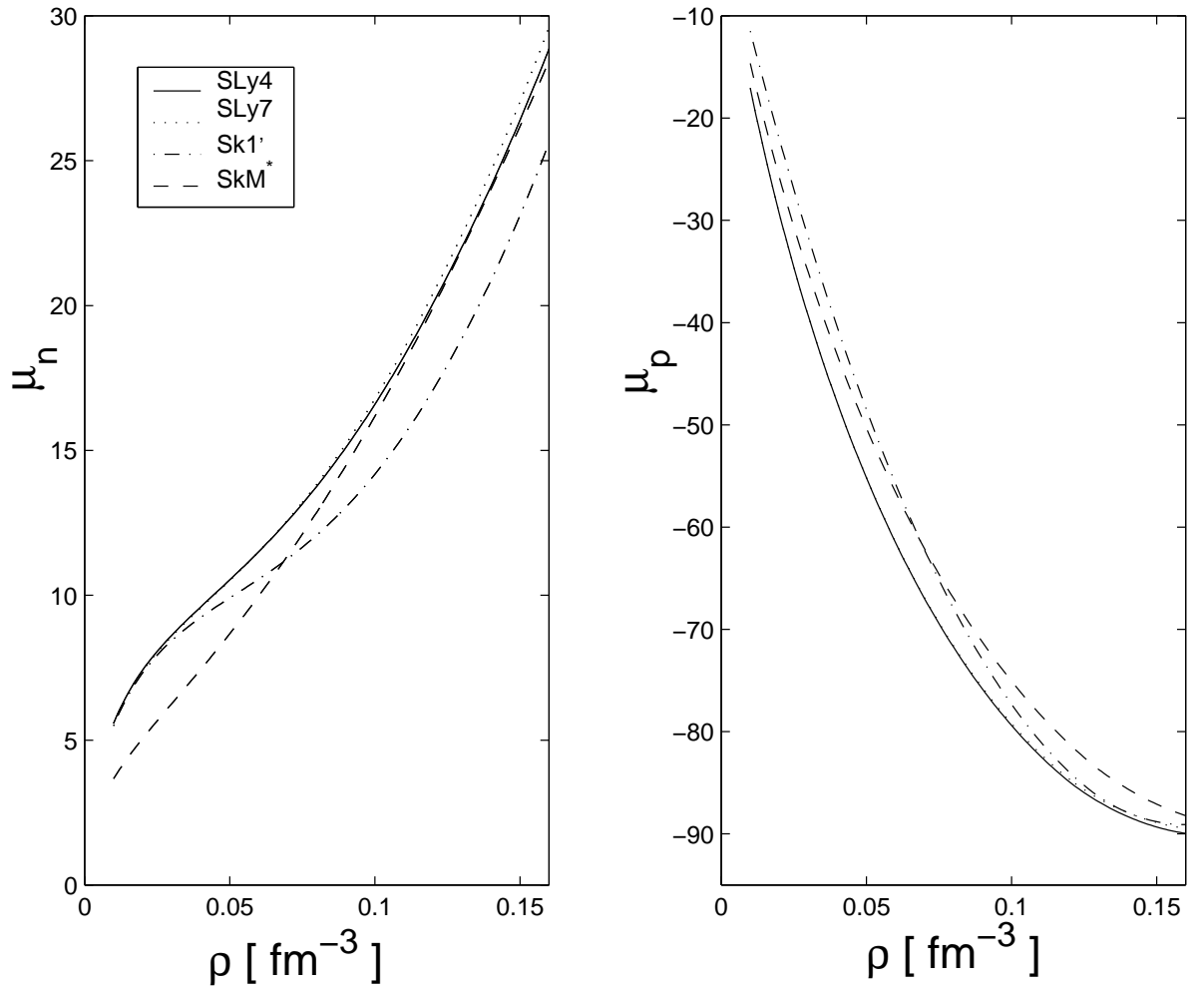


Figure 2:
 Neutron and proton chemical potentials (with rest energy subtracted), μ_n , μ_p , versus total nucleon density, ρ , for the SLy and SkM*, Sk1' forces, respectively. The μ_p curve for the SLy7 force cannot be graphically distinguished from the SLy4 one.

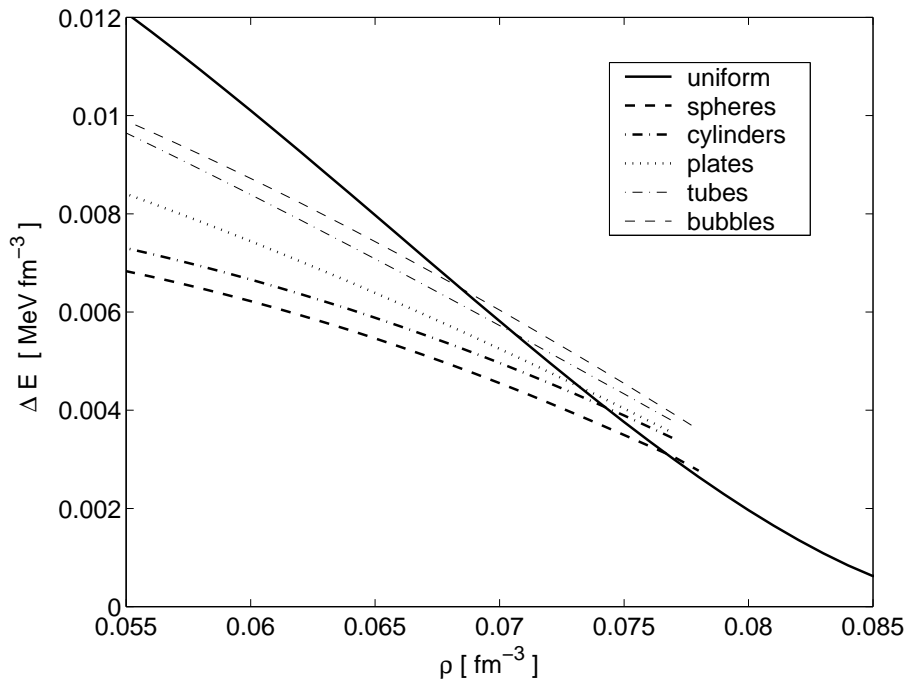


Figure 3:

Energy density of a given phase of inner-crust matter minus that of the bulk nuclear matter - neutron gas system, as a function of the average nucleon density, ρ . Thick solid line corresponds to the homogeneous npe matter. Calculations performed for the SLy4 force.

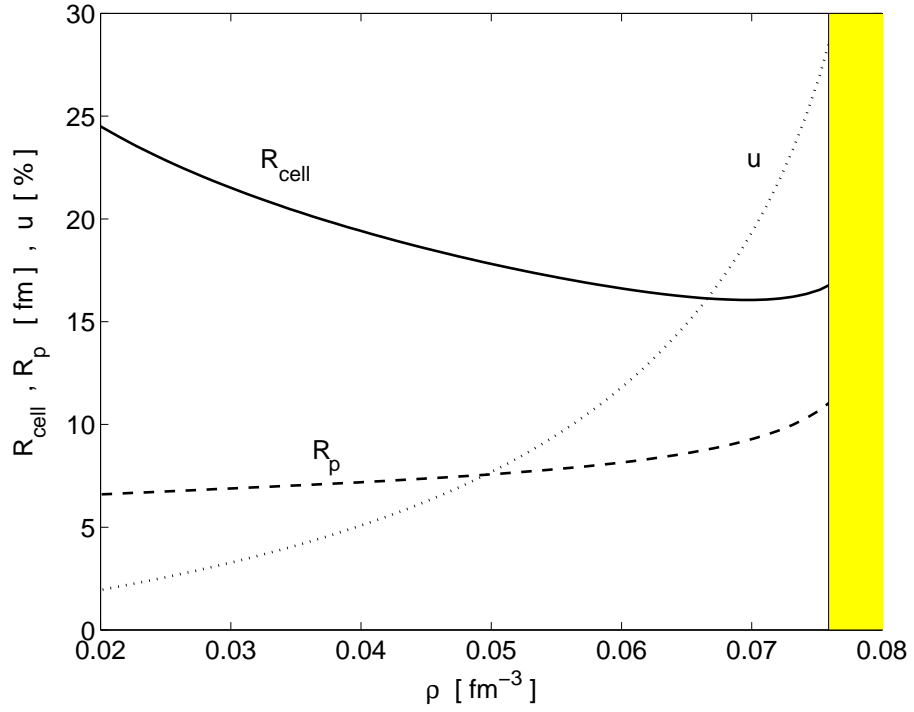


Figure 4:
 Radius of spherical Wigner-Seitz cell, R_{cell} , the proton radius of spherical nuclei, R_p , and fraction of volume filled by nuclear matter, u (in percent), versus average nucleon density, ρ . Shaded area corresponds to the homogeneous npe matter. Calculations performed for the SLy4 force.

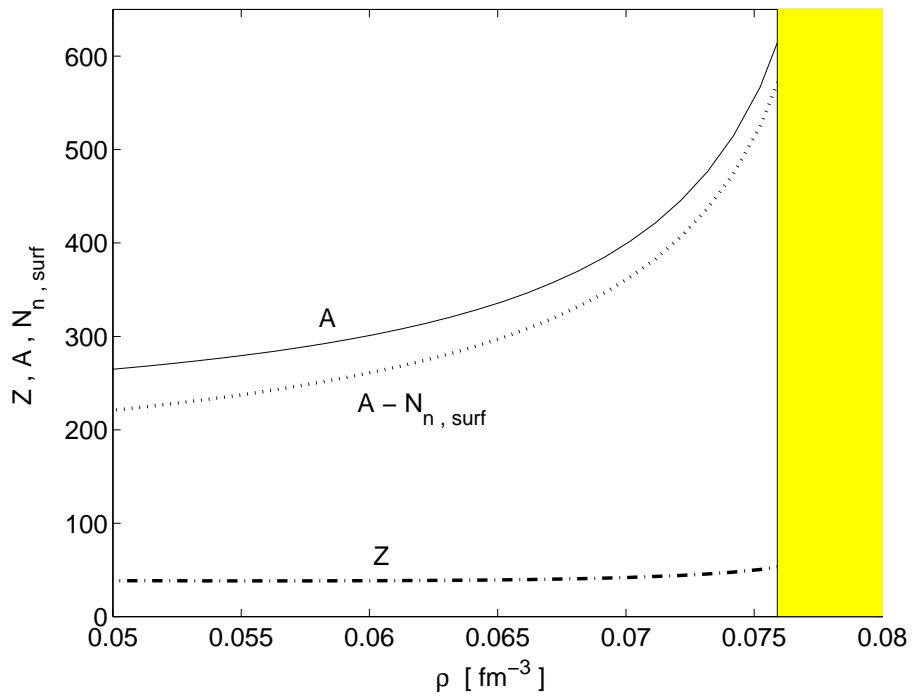


Figure 5:

Mass number of spherical nuclei, A , and their proton number, Z , versus average nucleon density, ρ . Dotted line corresponds to number of nucleons after deducing neutrons belonging to neutron skin. Shaded area corresponds to the homogeneous npe matter. Calculations performed for the SLy4 force.